MDMA doses of 2 mg/kg each leads one to question what distinguishes this particular drug regimen from the 4-day, twice daily, higher-dose regimen that engenders selective serotonergic neurotoxicity (*16*–*22*). One possibility is that the nonlinear pharmacokinetic profile of MDMA, such as that demonstrated in humans in the setting of closely spaced repeated dosing (*30*, *31*), leads to prolonged elevated brain levels of MDMA (or its metabolites) and that protracted exposure to MDMA renders dopamine neurons vulnerable to its toxic effects. An alternative (although not mutually exclusive) explanation is that repeated closely spaced doses of MDMA lead to higher elevations in body temperature, which is known to augment MDMA neurotoxicity (*32*). Additional studies are needed to evaluate these possibilities, in addition to alternative hypotheses.

In light of the present findings, and given the fact that MDMA use is widespread and increasing, one might ask why more cases of MDMA-induced Parkinsonism (*33*) have not been reported. There are multiple potential explanations, but only two will be mentioned. First, Parkinsonism does not generally become clinically apparent until more than 70 to 80% of brain dopamine has been depleted. Therefore, substantial MDMA-induced dopaminergic neurotoxicity could occur yet remain occult until unmasked by other processes (such as drug-induced interference with dopaminergic neurotransmission or decline in brain dopamine with advancing age). Second, until now, the potential for MDMA to damage brain dopamine neurons in primates has not been appreciated and, therefore, MDMA neurotoxicity has not been considered in the differential diagnosis of Parkinsonism in young adults. It is possible that some of the more recent cases of suspected young-onset Parkinson's disease might be related to MDMA exposure but that this link has not been recognized.

These findings suggest that humans who use repeated doses of MDMA over several hours are at high risk for incurring severe brain dopaminergic neural injury (along with significant serotonergic neurotoxicity). This injury, together with the decline in dopaminergic function known to occur with age (*15*), may put these individuals at increased risk for developing Parkinsonism and other neuropsychiatric diseases involving brain dopamine/serotonin deficiency, either as young adults or later in life.

References and Notes

1. L. D. Johnston, P. M. O'Malley, J. G. Bachman, *Monitoring the Future: National Survey Results on Drug Use, 1975–2000. Volume 1: Secondary School Students; Volume 2: College Students and Adults Ages 19–40* (NIH Publication Nos. 01-4924 and 01-4925, National Institute on Drug Abuse, Bethesda, MD, 2001).
2. European Monitoring Centre for Drugs and Drug Addiction (EMCDDA), *Annual Report on the State-of-the-Drug Problem in the European Union* (EMCDDA, Luxembourg, 2001), pp. 1–52.
3. S. J. Peroutka, *N. Engl. J. Med.* **317**, 1542 (1987).
4. E. Weir, *Can. Med. Assoc. J.* **162**, 1843 (2000).
5. A. C. Parrott, *Pharmacol. Biochem. Behav.* **71**, 837 (2002).
6. J. W. Gibb, G. R. Hanson, M. Johnson, in *Amphetamine and Its Analogs: Neuropsychopharmacology, Toxicology and Abuse*, A. Cho, D. Segal, Eds. (Academic Press, New York, 1994), pp. 269–295.
7. A. R. Green, A. J. Cross, G. M. Goodwin, *Psychopharmacology* **119**, 247 (1995).
8. G. A. Ricaurte, J. Yuan, U. D. McCann, *Neuropsychobiology* **42**, 5 (2000).
9. U. D. McCann, Z. Szabo, U. Scheffel, R. F. Dannals, G. A. Ricaurte, *Lancet* **352**, 1433 (1998).
10. A. C. Parrott, *Hum. Psychopharmacol. Clin. Exp.* **16**, 557 (2001).
11. E. O'Shea, B. Esteban, J. Camarero, A. R. Green, M. I. Colado, *Neuropharmacology* **40**, 65 (2001).
12. D. M. Stone, G. R. Hanson, J. W. Gibb, *Neuropharmacology* **26**, 1657 (1987).
13. Materials, methods, and data from NE and motor function studies are available as supporting material on *Science* Online.
14. R. P. Fink, L. Heimer, *Brain Res.* **4**, 369 (1967).
15. D. B. Calne, R. F. Peppard, *Can. J. Neurol. Sci.* **14** (suppl. 3), 424 (1987).
16. G. A. Ricaurte *et al., JAMA* **260**, 51 (1988).
17. T. R. Insel, G. Battaglia, J. N. Johannessen, S. Marra, E. B. DeSouza, *J. Pharmacol. Exp. Ther.* **249**, 713 (1989).
18. D. L. Frederick *et al., Neurotoxicol. Teratol.* **17**, 531 (1995).
19. K. T. Finnegan *et al., Brain Res.* **447**, 141 (1988).
20. G. A. Ricaurte, L. E. Delanney, I. Irwin, J. W. Langston, *Brain Res.* **446**, 165 (1988).
21. M. S. Kleven, W. L. Woolverton, L. S. Seiden, *Brain Res.* **488**, 121 (1989).
22. W. Slikker Jr. *et al., Toxicol. Appl. Pharmacol.* **94**, 448 (1988).
23. J. Mordenti, W. Chappell, in *Toxicokinetics in New Drug Development*, A. Yacobi, J. Kelly, V. Batra, Eds. (Pergamon, New York, 1989), pp. 42–96.
24. U. D. McCann, M. Mertl, V. Eligulashvili, G. A. Ricaurte, *Psychopharmacology* **143**, 417 (1999).
25. M. J. Morgan, *Psychopharmacology* **141**, 30 (1999).
26. E. Gouzoulis-Mayfrank *et al., J. Neurol. Neurosurg. Psychiatry* **68**, 719 (2000).
27. I. Elayan *et al., Eur. J. Pharmacol.* **221**, 281 (1992).
28. Z. Zhao, N. Castagnoli, G. A. Ricaurte, T. Steele, M. B. Martello, *Chem. Res. Toxicol.* **5**, 89 (1992).
29. M. Johnson *et al., J. Pharmacol. Exp. Ther.* **261**, 447 (1992).
30. R. de la Torre *et al., Br. J. Clin. Pharmacol.* **49**, 104 (2000).
31. M. Farré *et al., Drug Alcohol Depend.* **63** (suppl. 1), S46 (2001).
32. J. E. Malberg, L. S. Seiden, *J. Neurosci.* **18**, 5086 (1998).
33. S. Mintzer, S. Hickenbottom, S. Gilman, *N. Engl. J. Med.* **340**, 1443 (1999).

34. We thank C. Bentley for her assistance in preparing the manuscript and M. Kilbourne for kindly supplying [^{3}H]methoxytetrabenazine. Supported by USPHS grants DA 5707, DA 13790, DA 09487, DA 00206, and DA 10217.

Supporting Online Material

www.sciencemag.org/cgi/content/full/297/5590/2260/DC1
Materials and Methods
Figs. S1 to S3
References and Notes

29 May 2002; accepted 14 August 2002

Conversion of Unc104/KIF1A Kinesin into a Processive Motor After Dimerization

Michio Tomishige, Dieter R. Klopfenstein, Ronald D. Vale*

Unc104/KIF1A belongs to a class of monomeric kinesin motors that have been thought to possess an unusual motility mechanism. Unlike the unidirectional motion driven by the coordinated actions of the two heads in conventional kinesins, single-headed KIF1A was reported to undergo biased diffusional motion along microtubules. Here, we show that Unc104/KIF1A can dimerize and move unidirectionally and processively with rapid velocities characteristic of transport in living cells. These results suggest that Unc104/KIF1A operates in vivo by a mechanism similar to conventional kinesin and that regulation of motor dimerization may be used to control transport by this class of kinesins.

Caenorhabditis elegans Unc104 and the mouse ortholog KIF1A are kinesin motors that transport synaptic vesicle precursors along microtubules from the neuronal cell body to the nerve terminal (*1*–*3*). For such long-range transport to be efficient, organelles that encounter a microtubule must move processively. Conventional kinesin, which belongs to a different subfamily of vesicle-transporting kinesins, is dimeric and uses its two motor domains in a coordinated manner to take successive, unidirectional 8-nm steps along the microtubule without dissociating (*4*). However, KIF1A (*2*) and Unc104 (*5*) are monomeric in solution and are thought to operate using a different motility mechanism, because a single KIF1A motor domain has been shown to undergo biased diffusional movement along the microtubule (*6*). A novel processivity mechanism was proposed that involves an electro-

The Howard Hughes Medical Institute and the Department of Cellular and Molecular Pharmacology, University of California, San Francisco, CA 94143, USA.

*To whom correspondence should be addressed. E-mail: vale@phy.ucsf.edu

static interaction between a highly basic loop (the K loop) on the motor domain and the disordered, negatively charged COOH-terminus of tubulin (*7*, *8*); a nucleotide-induced rotation of the motor domain is believed to create directional bias (*9*). However, the observed net motion (0.14 μm/s) (*6*) is ~eight times slower than that observed for full-length Unc104/KIF1A-induced movement in vivo (*3*) and in vitro (*2*). In addition, biased diffusion was not observed for the *C. elegans* Unc104 motor domain (*5*) and may be an artifact of particular motor constructs and buffer condition (*10*). Hence, the normal mode of motility for this kinesin class [often referred to as the "monomeric" kinesins (*11*)] has not been clear (*12*).

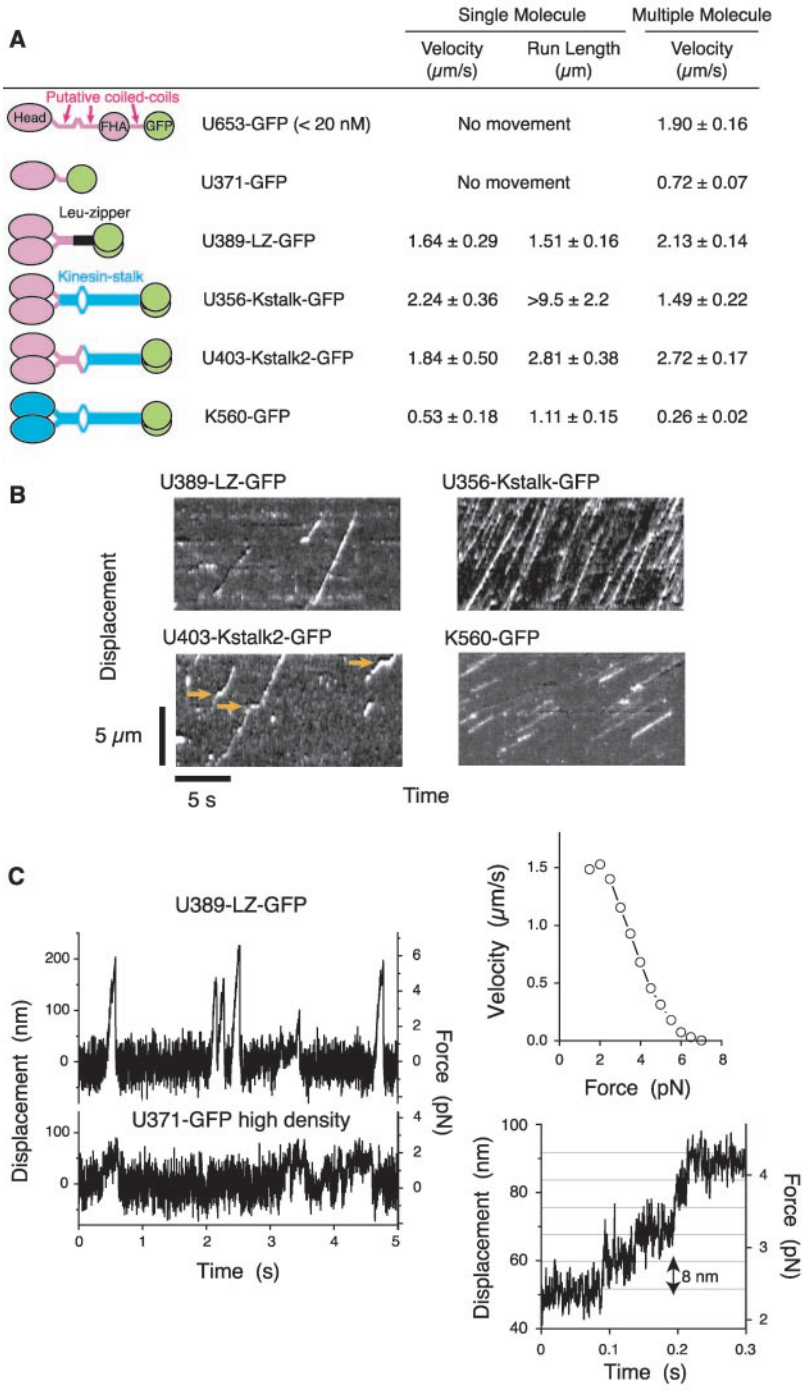

Fig. 1. Single-molecule motility of artificially dimerized Unc104-GFP. (**A**) Single-molecule velocities and run lengths were measured with TIRF microscopy (at <20 nM motor concentrations), and multiple-molecule velocities were determined with a microtubule gliding assay (*21*). The velocity of U403-Kstalk2-GFP was determined during the portions of traces without pauses. See (*14*) for further details. (**B**) Kymographs showing frequency, velocity, and processivity of dimerized Unc104 constructs and a conventional kinesin construct (K560-GFP) along axonemes. Unidirectional movement appears in this plot as a diagonal line. Arrows show transient pauses during movement of U403-Kstalk2-GFP. (**C**) The movement of a bead coated with U389-LZ-GFP at predicted single motor density and U371-GFP at 100-fold higher motor density at 1 mM ATP in an optical trap (*14*) (left), the force-velocity curve of U389-LZ-GFP (upper right), and a raw trace of a U389-LZ-GFP–coated bead at 10 μM ATP showing successive ~8-nm steps (lower right).

Sequence analysis of Unc104/KIF1A (and other members of this kinesin class) revealed potential coiled-coil regions adjacent to the motor domain, the first of which aligns with the neck coiled-coil of conventional kinesin (*11*), a region believed to play a role in head-head coordination (*4*). However, the probability of coiled-coil formation is low and may require high motor concentrations for dimerization. We recently found that concentration of Unc104 into lipid rafts facilitated liposome transport along microtubules and that a mutation predicted to destabilize the neck coiled-coil inhibited liposome movement (*13*). Collectively, these findings raised the possibility that Unc104/KIF1A might dimerize and operate by a two-headed mechanism, and we sought to test this idea using single-molecule analyses.

Our hypothesis predicted that constitutively dimerized Unc104/KIF1A motors would show processive unidirectional motion along the microtubule and not biased diffusion. We created two constitutive Unc104 dimers [green fluorescent protein (GFP)–tagged] either by fusing the GCN4 leucine zipper (LZ) after the proposed Unc104 neck coiled-coil (U389-LZ-GFP) or by joining the kinesin neck coiled-coil and stalk to Unc104 motor domain (U356-Kstalk-GFP) (Fig. 1A) (*14*). In contrast to two monomeric Unc104 constructs (U653-GFP and U371-GFP), the two constitutive Unc104 dimers showed robust processive movement that was smooth and unidirectional in a single-molecule, total internal reflection fluorescence (TIRF) motility assay (Fig. 1B and movie S1). The run lengths were several microns long, which is comparable to or greater than those reported for conventional kinesin (Fig. 1A), and the velocities were similar to those measured for Unc104 in the gliding assay (Fig. 1A) (*5*) and in vivo (*3*). It was previously suggested that the fast velocities produced by Unc104/KIF1A (three- to fourfold greater than those produced by conventional kinesin) required many motors interacting simultaneously with a microtubule (*5*, *15*). However, our results indicate that these fast velocities are intrinsic to the motor domains of a single dimerized Unc104 molecule (*16*).

Because the GCN4 region of U389-LZ-GFP could induce coiled-coil formation in the adjacent Unc104 sequence, another dimeric Unc104 was created that separated the putative Unc104 neck coiled-coil and the

kinesin stalk with a ~35–amino acid unstructured region. This U403-Kstalk2-GFP protein showed unidirectional movement with a similar velocity to U389-LZ-GFP (Fig. 1A), suggesting that the Unc104 neck can form a coiled-coil. However, unlike U389-LZ-GFP, U403-Kstalk2-GFP often paused during the movement (Fig. 1B, arrows), possibly due to a temporary unwinding of the native Unc104 neck coiled-coil.

Using an optical trap, we also measured the mechanical properties of single U389-LZ-GFP molecules attached to 1-μm beads. U389-LZ-GFP displayed a linear force-velocity curve, stalled when opposed by a force of ~6 pN, and displayed 8-nm steps (Fig. 1C). These mechanical properties are similar to those of conventional kinesin (*17*), implying a similar motility mechanism. In contrast, U371-GFP, which had most of the coiled-coil region removed, did not show movement at single-molecule densities. At 10- to 100-fold higher motor densities, U371-GFP–coated beads moved, but the stall forces (<3 pN) and velocities (<0.6 μm/s) were both low (Fig. 1C). These results reveal that many truncated monomers can work cooperatively to move a cargo, but the stall forces and velocities are lower than those produced by a single dimer.

To test whether coiled-coil formation in the Unc104 neck region is required for processivity, we used a mutant in which two hydrophobic residues in the first predicted heptad repeat were changed to charged residues [Ile^{362} to Glu^{362} and Leu^{365} to Lys^{365} (I362E/L365K) (Fig. 2A)] (*13*, *18*). This neck destabilization mutation in U653-GFP and U403-Kstalk2-GFP decreased the velocity of microtubule gliding to closer to that of U371-GFP (Fig. 2B), suggesting conversion to a monomer mechanism. Consistent with this idea, this mutation abolished the unidirectional movement of single U403-Kstalk2-GFP molecules, which instead showed diffusional movement with a small plus-end–directed bias (Fig. 2C). This mutation had no effect on the gliding velocity of U371-GFP (Fig. 2B), indicating that the catalytic core was not affected. These observations reveal that coiled-coil formation in the neck region is required for head-head coordination in an Unc104 dimer, as is true for conventional kinesin.

Previous studies with a native construct (U653-GFP) reported no processive movement (*5*); however, these single-molecule assays require low concentrations (<20 nM) of fluorescently labeled motor to reduce background fluorescence, which may be incompatible with motor dimerization because of the low coiled-coil probability (*19*). Supporting the idea that U653 might form dimers at higher concentrations (3 μM), we observed dimeric U653 species by SDS–polyacrylamide gel electrophoresis (SDS-PAGE) after addition of a zero-length chemical crosslinker (Fig. 3A). To test whether U653 might dimerize into a processive motor, we increased the motor concentration in the single-molecule fluorescence assay without increasing the background fluorescence by adding an excess of non-GFP–labeled U653 (0.1 to 7 μM) to a fixed concentration of GFP-tagged motor (7 nM). With >1 μM "dark" motor, single U653-GFP molecules now showed fast unidirectional movement (Fig. 3, B and C, and movie S2) with movement properties (table S1) nearly identical to those of the artificially dimerized Unc104 motors (Fig. 1A). In contrast, the movement frequency of conventional kinesin (K560-GFP) did not increase upon addition of dark motor (K560) (Fig. 3B), and the monomer U371-GFP never moved unidirectionally even after addition of 7 μM dark U371 (Fig. 3B) or U653 (not shown). We also obtained similar results using rat KIF1A (fig. S1 and movie S3).

To confirm that high motor concentrations cause dimerization through the Unc104 stalk region, we made a chimeric motor consisting of the motor domain of conventional kinesin fused to the coiled-coils and the forkhead-associated (FHA) domain of Unc104 (termed K336-Ustalk-GFP). At low concentrations, this chimeric motor did not move, but upon addition of >1 μM of dark K336-Ustalk, processive movement occurred at a rate characteristic of conventional kinesin (Fig. 3C and table S1). Processivity of conventional kinesin requires dimerization (*4*), which in this case must be mediated by the Unc104 sequence. When non-GFP–labeled U653 was added to GFP-labeled K336-Ustalk, we also observed processive movement of GFP-labeled motors but at a higher velocity of 0.78 μm/s as compared to the velocity after the addition of K336-Ustalk (*P* value of 10^{-10}) (Fig. 3C). This higher velocity is most likely due to a heterodimer composed of a conventional kinesin motor domain and an Unc104 motor domain joined by an Unc104 stalk (additional information in table S1).

To examine whether a single dimeric Unc104 is sufficient to move membranes processively along microtubules, we used an in vitro vesicle transport assay in which U653-GFP-His_6 molecules were bound to 1-μm-diameter liposomes containing 10% Ni–nitrilotriacetic acid (NTA)–conjugated lipid. This provided a stronger motor-membrane attachment than the Unc104-phosphoinositide interaction that we described previously (*13*). The Ni-NTA–containing liposomes moved smoothly along microtubules at veloc-

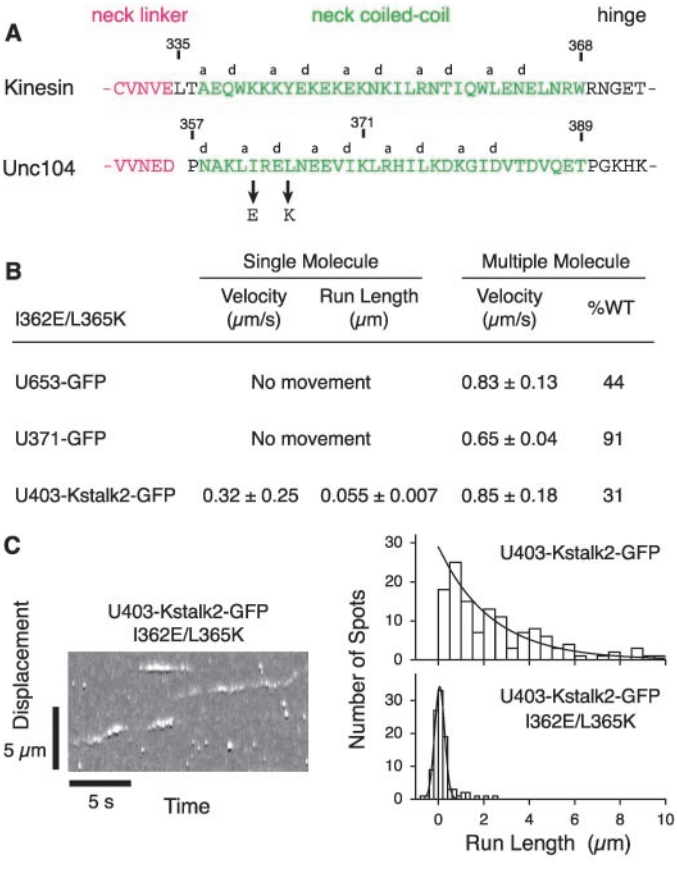

Fig. 2. A neck coiled-coil destabilizing mutation inhibits the fast velocity and processivity of Unc104. (**A**) Sequence alignments of human conventional kinesin and *C. elegans* Unc104 reveal a putative neck coiled-coil sequence in Unc104 (*a* and *d* positions of heptad repeats are shown). Single-letter abbreviations for the amino acid residues are as follows: A, Ala; C, Cys; D, Asp; E, Glu; F, Phe; G, Gly; H, His; I, Ile; K, Lys; L, Leu; M, Met; N, Asn; P, Pro; Q, Gln; R, Arg; S, Ser; T, Thr; V, Val; W, Trp; and Y, Tyr. (**B**) Single-molecule velocities, run lengths [derived from the Gaussian fit shown in (C)], and microtubule-gliding velocities of the neck destabilizing mutation (I362E/L365K) are shown in the constructs depicted in Fig. 1A. (**C**) Kymograph of U403-Kstalk2-GFP I362E/L365K showing diffusional movements (left) and run length distributions of U403-Kstalk2-GFP without and with I362E/L365K mutation (*14*) (right).

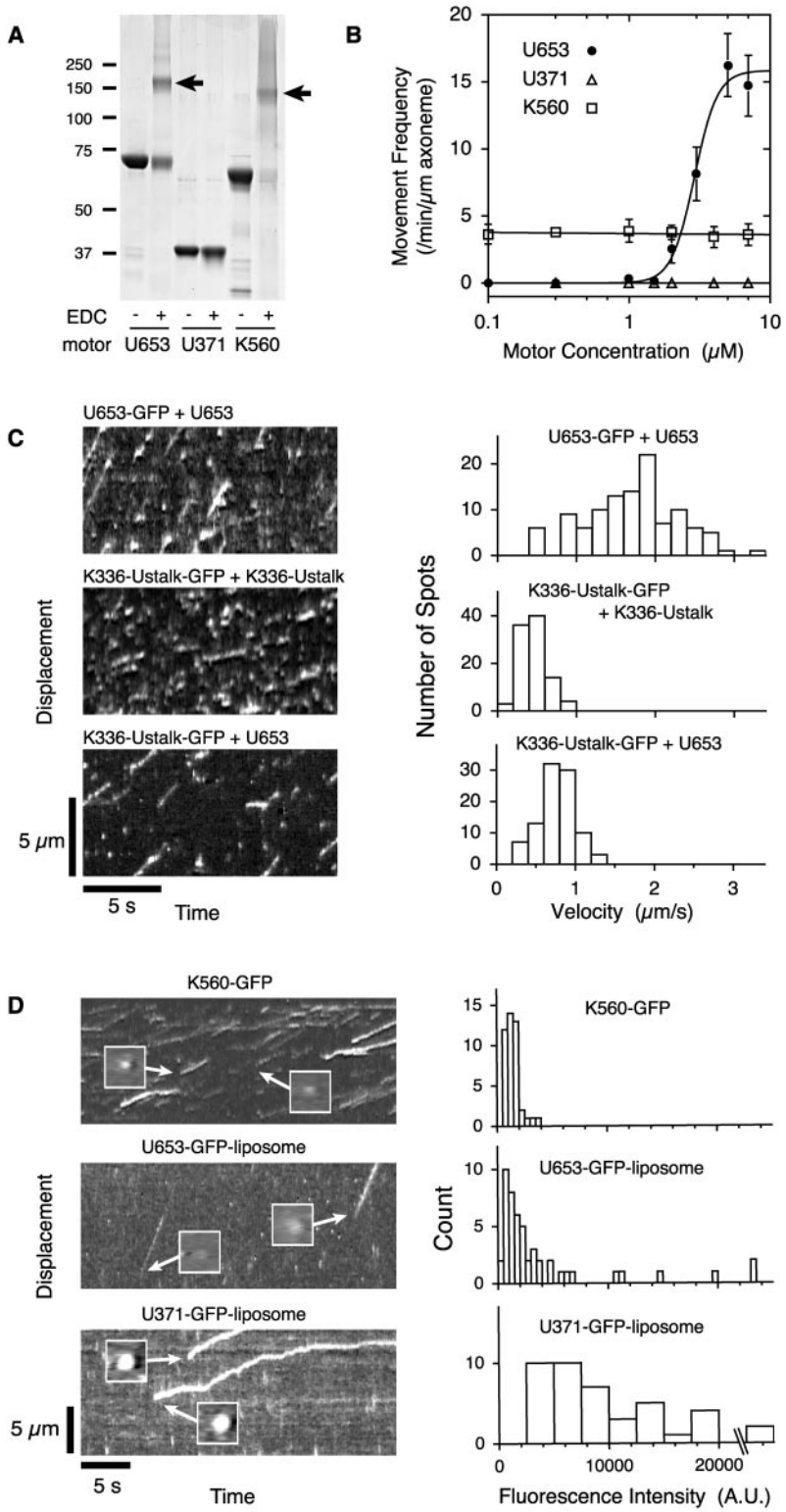

Fig. 3. Fast processive movement of single U653-GFP motors at high motor concentrations. (**A**) SDS-PAGE after treatment of 3 μM U653, U371, and K560 with and without the zero-length cross-linker 1-ethyl-3-(3-dimethylaminopropyl)carbodiimide (EDC). Arrows show the U653 and K560 dimers. U371 did not cross-link into a dimer-sized band. (**B**) Frequencies of the movement of U653-GFP, U371-GFP, and K560-GFP (at 7 nM) along axonemes as a function of concentration of added non–GFP-labeled motors. (**C**) Kymographs showing unidirectional movements (left) and distributions of velocities (right) of U653-GFP with 2 μM dark U653, K336-Ustalk-GFP with 2 μM dark K336-Ustalk, and K336-Ustalk-GFP with 2 μM dark U653 (also see table S1). (**D**) Kymographs (left) and distributions of spot intensities (right) of Ni-NTA liposomes transported by U653- or U371-GFP-His_6, and of K560-GFP (the latter without liposomes) moving along axonemes visualized with TIRF microscopy. Insets in the kymograph show fluorescence images of the moving liposomes (or K560-GFP alone). A.U., arbitrary units.

ities of 1.68 ± 0.14 μm/s. We then measured the number of U653 molecules spanning between moving liposomes and the microtubule using TIRF microscopy. Although several GFP-tagged U653 molecules may be bound to the 1-μm liposomes, only the molecules within ~150 nm of the slide can be clearly visualized in the evanescent field. The fluorescence intensities of moving U653-GFP-liposomes varied, but the minimum intensity peak was similar to that of single conventional kinesin molecules tagged with GFP (Fig. 3D and movie S4). In contrast, the truncated monomer U371-GFP-His_6 supported liposome movement only at three- to fourfold higher motor concentrations than U653-GFP-His_6 motor concentrations, and these moving liposomes displayed higher fluorescence intensities and slower velocities (0.38 ± 0.09 μm/s) with frequent pausing (Fig. 3D and movie S5). These findings suggest that many monomers are required to move a vesicle, but a single U653 dimer can transport a membrane at maximal velocity.

The positively charged K loop on the motor domain was reported to be essential for the biased diffusion of monomeric KIF1A (*7*, *8*). When the K loop of U356-Kstalk-GFP was replaced with the noncharged loop of conventional kinesin (K0), processive movement was observed with velocities similar to that of the wild type (WT) (WT and K0, 2.24 ± 0.36 and 1.72 ± 0.52 μm/s, respectively), but the run lengths were dramatically decreased (WT and K0, >9.5 ± 2.2 and 1.75 ± 0.12 μm, respectively) (fig. S2, A to C). The maximum force produced by the K0 mutant was within 15% of that of the wild type (fig. S2D). Therefore, in dimeric Unc104, the K loop is not needed for either processivity or force production but enhances the run length under low load conditions, as has been described for positively charged residues in the neck coiled-coil of conventional kinesin (*20*).

We have shown that Unc104/KIF1A can dimerize through a weak coiled-coil region and that upon dimerization, single Unc104/KIF1A molecules move processively along microtubules. The processive mechanism of dimeric Unc104/KIF1A appears to be similar to that of conventional kinesin, except that the long run length of Unc104/KIF1A is reliant on its unique microtubule-binding K loop. Because single Unc104/KIF1A dimers move at the maximal velocities recorded for this motor in vivo, we propose that Unc104/KIF1A transports its cargo as dimers in living cells. Dimer-driven vesicle transport in vitro is also smoother, faster, and more efficient than that driven by many monomeric motors with low duty ratios. Our findings also imply that cargo motility by this "monomeric" class of motors can be regulated by promoting or inhibiting the transition to a functional dimer. This transition may be facili-

tated by concentrating motors into lipid raft domains (*13*) or by enhancing neck coiled-coil stability, possibly by factors binding to the FHA domain located adjacent to the Unc104/KIF1A neck coiled-coil (fig. S3).

References and Notes

1. A. J. Otsuka *et al., Neuron* **6**, 113 (1991).
2. Y. Okada, H. Yamazaki, Y. Sekine-Aizawa, N. Hirokawa, *Cell* **81**, 769 (1995).
3. H. M. Zhou, I. Brust-Mascher, J. M. Scholey, *J. Neurosci.* **21**, 3749 (2001).
4. R. D. Vale, R. A. Milligan, *Science* **288**, 88 (2000).
5. D. W. Pierce, N. Hom-Booher, A. J. Otsuka, R. D. Vale, *Biochemistry* **38**, 5412 (1999).
6. Y. Okada, N. Hirokawa, *Science* **283**, 1152 (1999).
7. _____, *Proc. Natl. Acad. Sci. U.S.A.* **97**, 640 (2000).
8. M. Kikkawa, Y. Okada, N. Hirokawa, *Cell* **100**, 241 (2000).
9. M. Kikkawa *et al.*, *Nature* **411**, 439 (2001).
10. In our assays, neither the dimeric Unc104 motors nor the truncated monomers (U362-GFP or U371-GFP) displayed the biased diffusional motion reported by Okada and Hirokawa (*6*, *7*). However, we were able to observe this motion only by adding extra positively charged residues to the neck linker region and under specific buffer condition (see movie S6 legend for details).
11. R. D. Vale, R. J. Fletterick, *Annu. Rev. Cell Dev. Biol.* **13**, 745 (1997).
12. G. S. Bloom, *Curr. Opin. Cell Biol.* **13**, 36 (2001).
13. D. R. Klopfenstein, M. Tomishige, N. Stuurman, R. D. Vale, *Cell* **109**, 347 (2002).
14. Materials and methods are available as supporting material on *Science* Online.
15. K. R. Rogers *et al.*, *EMBO J.* **20**, 5101 (2001).
16. To achieve motility velocities of 2 μm/s with an 8-nm step size, one would predict an adenosine triphosphatase catalytic rate constant of ~125 adenosine 5′-triphosphate (ATP)/s per head for the constitutive Unc104 dimers. Our measured rates varied depending on the protein preparation but were in the range of 30 to 100 ATP/s per head, suggesting that some portion of the molecules may be inactive. The microtubule concentration for half-maximal ATPase stimulation of U356-Kstalk-GFP (0.078 μM) was two orders of magnitude smaller than that of U653 (*5*), indicating an increased microtubule affinity.
17. K. Svoboda, S. M. Block, *Cell* **77**, 773 (1994).
18. The I362E/L365K mutation is predicted to decrease the probability of coiled-coil formation in Unc104's neck coiled-coil from 0.22 to 0.002 (using the computer program COILS version 2.2) but not to change probabilities of the other two coiled-coils (405 to 451 and 595 to 651 amino acids). The chemical cross-linking experiment (*14*) showed that U403-Kstalk2-GFP containing the I362E/L365K mutation was still a dimer (*22*).
19. KIF1C, a member of the Unc104/KIF1 subfamily, has been shown to dimerize in fibroblasts overexpressing KIF1C, but not under physiological conditions (*23*).
20. K. S. Thorn, J. A. Ubersax, R. D. Vale, *J. Cell Biol.* **151**, 1093 (2000).
21. M. Tomishige, R. D. Vale, *J. Cell Biol.* **151**, 1081 (2000).
22. Data not shown.
23. C. Dorner, A. Ullrich, H.-U. Haring, R. Lammers, *J. Biol. Chem.* **274**, 33654 (1999).

24. We thank U. Wiedemann for support in cloning, N. Stuurman and Y. Cui for helpful discussions, and B. Schnapp for providing rat KIF1A cDNA. Supported by grants from the Howard Hughes Medical Institute and NIH (grant AR42895).

Supporting Online Material

www.sciencemag.org/cgi/content/full/297/5590/2263/DC1
Materials and Methods
Figs. S1 to S3
Table S1
References
Movies S1 to S6

29 April 2002; accepted 8 August 2002

Role of Hec1 in Spindle Checkpoint Signaling and Kinetochore Recruitment of Mad1/Mad2

Silvia Martin-Lluesma, Volker M. Stucke, Erich A. Nigg*

The spindle checkpoint delays sister chromatid separation until all chromosomes have undergone bipolar spindle attachment. Checkpoint failure may result in chromosome mis-segregation and may contribute to tumorigenesis. We showed that the human protein Hec1 was required for the recruitment of Mps1 kinase and Mad1/Mad2 complexes to kinetochores. Depletion of Hec1 impaired chromosome congression and caused persistent activation of the spindle checkpoint, indicating that high steady-state levels of Mad1/Mad2 complexes at kinetochores were not essential for checkpoint signaling. Simultaneous depletion of Hec1 and Mad2 caused catastrophic mitotic exit, making Hec1 an attractive target for the selective elimination of spindle checkpoint–deficient cells.

The genomic stability of all organisms depends on the correct segregation of chromosomes during cell division (*1*, *2*). The accuracy of this process is monitored by the spindle assembly checkpoint (*3*, *4*). This surveillance mechanism is able to detect a single unaligned chromosome, causing a prometaphase arrest until proper bipolar attachment is achieved (*5*). First identified in yeast, several core checkpoint components have also been characterized in multicellular organisms (*6*–*9*). In humans, these include the protein kinases Bub1, BubR1, Mps1, the Bub1/R1-partner Bub3 (*10*, *11*), and the Mad1/Mad2 complex (*12*, *13*). All these proteins localize to kinetochores, particularly during early stages of mitosis (*3*). The prevailing model of spindle checkpoint function holds that the absence of an appropriate kinetochore–microtubule (MT) interaction generates a signal that inhibits the activity of a ubiquitin ligase termed anaphase-promoting complex/cyclosome (APC/C). In turn, APC/C activates the proteolytic degradation of securin, an inhibitor of sister chromatid separation (*2*). Both Mad2 (*14*–*16*) and multiprotein complexes comprising Mad2, BubR1, and Bub3 (*17*, *18*) have been implicated in the inhibition of APC/C. Upon proper attachment of the last kinetochore, the APC/C-inhibitory signal is extinguished, and anaphase ensues.

At the heart of this model, two key questions need to be answered. First, how is a cell cycle–inhibitory signal generated at unattached kinetochores, and second, how is this signal extinguished upon attachment of the last kinetochore? Early models for the generation of an inhibitory signal have emphasized the importance of a transient association of a Mad1/Mad2 complex with unattached kinetochores. Conversely, the loss of Mad2 from kinetochores has been correlated with checkpoint silencing (*4*, *19*). However, the kinetochore association of checkpoint components may depend on whether tension and/or MT attachment is impaired at the kinetochore (*3*, *20*, *21*). Furthermore, soluble APC/C-inhibitory complexes exist already in interphase cells before kinetochore assembly (*17*).

In a yeast two-hybrid screen for human Mad1-interacting proteins (*22*), we isolated a cDNA coding for full-length human Hec1 (highly expressed in cancer) (*23*) (fig. S1A). This coiled-coil protein is a putative mammalian homolog of budding yeast Ndc80p (*24*). The exact functions of Hec1 and Ndc80p are unknown, but both proteins localize to kinetochores (*23*, *25*). Yeast Ndc80p forms a complex with kinetochore proteins Nuf2p, Spc24p, and Spc25p, and mutational inactivation of these components causes defects in chromosome segregation (*25*–*27*). Similarly, microinjection of antibodies to Hec1 into mammalian cells disrupts mitotic progression (*23*). As shown by immunofluorescence microscopy, Hec1 was present on kinetochores throughout mitosis (fig. S1B) (*23, 25*), whereas Mad1 was released upon alignment of chromosomes at the metaphase plate (fig. S1B) (*28*). Mapping of the Hec1 and Mad2 binding sites on Mad1 revealed them to be distinct, indicating that Mad1 could bind both proteins simultaneously (fig. S1A).

To directly explore the functional significance of the Hec1–Mad1 interaction in HeLa S3 cells, gene silencing by small interfering RNA (siRNA) was used (*29*). Immunofluorescence microscopy (Fig. 1A and fig. S2)

Department of Cell Biology, Max-Planck-Institute of Biochemistry, Am Klopferspitz 18a, D-82152 Martinsried, Germany.

*To whom correspondence should be addressed. E-mail: nigg@biochem.mpg.de